AFRL-AFOSR-VA-TR-2023-0184

Passive Multidimensional Imaging and Recognition with Multiple Degrees of Freedom

Javidi, Bahram
UNIVERSITY OF CONNECTICUT
438 WHITNEY RD EXTENSION UNIT 1133
STORRS, CT, 06269
USA

11/18/2022
Final Technical Report

DISTRIBUTION A: Distribution approved for public release.

Air Force Research Laboratory
Air Force Office of Scientific Research
Arlington, Virginia 22203
Air Force Materiel Command

DISTRIBUTION A: Distribution approved for public release.

REPORT DOCUMENTATION PAGE

PLEASE DO NOT RETURN YOUR FORM TO THE ABOVE ORGANIZATION.

1. REPORT DATE	2. REPORT TYPE	3. DATES COVERED	
20221118	Final	START DATE 20180615	END DATE 20220831

4. TITLE AND SUBTITLE
Passive Multidimensional Imaging and Recognition with Multiple Degrees of Freedom

5a. CONTRACT NUMBER	5b. GRANT NUMBER	5c. PROGRAM ELEMENT NUMBER
	FA9550-18-1-0338	61102F
5d. PROJECT NUMBER	**5e. TASK NUMBER**	**5f. WORK UNIT NUMBER**

6. AUTHOR(S)
Bahram Javidi

7. PERFORMING ORGANIZATION NAME(S) AND ADDRESS(ES)
UNIVERSITY OF CONNECTICUT
438 WHITNEY RD EXTENSION UNIT 1133
STORRS, CT 06269
USA

8. PERFORMING ORGANIZATION REPORT NUMBER

9. SPONSORING/MONITORING AGENCY NAME(S) AND ADDRESS(ES)	10. SPONSOR/MONITOR'S ACRONYM(S)	11. SPONSOR/MONITOR'S REPORT NUMBER(S)
Air Force Office of Scientific Research 875 N. Randolph St. Room 3112 Arlington, VA 22203	AFRL/AFOSR RTB1	AFRL-AFOSR-VA-TR-2023-0184

12. DISTRIBUTION/AVAILABILITY STATEMENT
A Distribution Unlimited: PB Public Release

13. SUPPLEMENTARY NOTES

14. ABSTRACT
The purpose of this project is to introduce, investigate, and demonstrate a new multi-dimensional sensing capability where a small number of photons may allow the possibility of implementing reliable multidimensional visualization, identification, and classification using polarimetric and multi-spectral band passive imaging. The multi-dimensional sensing and imaging proposed here are intended to operate under extremely sparse (low photon count) data conditions to enable many benefits, including operation in degraded environments, removing of occlusion to allow visualization of occluded objects, multi-dimensional target recognition, and tracking of occluded objects. Unlike LADAR, which uses active illumination to measure time of flight, this passive multi-dimensional sensing approach uses 2D image sensors with ambient light or thermal imaging for persistent and covert operation. This capability will be very beneficial to enhancing surveillance, monitoring human activities, and information exploitation. During the course of this project, we have performed experiments and theoretical analysis of the objectives and tasks of the project. We have investigated polarimetric multidimensional imaging in degraded environments. The polarization state of light contains optical and physical properties of the scene. Compared with conventional imaging, polarimetric imaging can reveal additional information about the scene, and it has the potential for material inspection and classification in various applications. We have investigated deep convolutional neural network model [1-5] using physics based training with three-dimensional (3D) imaging to recognize polarimetric 3D objects in degraded environments such as low light and partial occlusions [2].

15. SUBJECT TERMS

16. SECURITY CLASSIFICATION OF:			17. LIMITATION OF ABSTRACT	18. NUMBER OF PAGES
a. REPORT U	b. ABSTRACT U	c. THIS PAGE U	UU	26

19a. NAME OF RESPONSIBLE PERSON	19b. PHONE NUMBER *(Include area code)*
MICHAEL YAKES	00000000

DISTRIBUTION A: Distribution approved for public release.

AFOSR Final Report (2018-2022)

Sponsor Name: Air Force Office of Scientific Research

Project Title: Passive Multidimensional Imaging and Recognition with Multiple Degrees of Freedom under Fixed Resource Constraints

AWARD NO. FA9550-18-1-0338

Period Start: 15-June-2018
Period End: 31-August-2022

PI/Technical POC: **Prof. Bahram Javidi**, Principal Investigator
Electrical and Computer Engineering Department
University of Connecticut, 371 Fairfield Rd., U-4157,
Storrs, CT 06269-4157
Email: bahram.javidi@uconn.edu

Program Manager: Dr. Michael Yakes
Air Force Office of Scientific Research
875 North Randolph Street
Arlington, VA 22203
Email: michael.yakes@us.af.mil

DISTRIBUTION A: Distribution approved for public release.

Prof. Bahram Javidi, University of Connecticut; Email: Bahram.Javidi@UConn.edu

Report Abstract

The purpose of this project is to introduce, investigate, and demonstrate a new multi-dimensional sensing capability where a small number of photons may allow the possibility of implementing reliable multidimensional visualization, identification, and classification using polarimetric and multi-spectral band passive imaging. The multi-dimensional sensing and imaging proposed here are intended to operate under extremely sparse (low photon count) data conditions to enable many benefits, including operation in degraded environments, removing of occlusion to allow visualization of occluded objects, multi-dimensional target recognition, and tracking of occluded objects. Unlike LADAR, which uses active illumination to measure time of flight, this passive multi-dimensional sensing approach uses 2D image sensors with ambient light or thermal imaging for persistent and covert operation. This capability will be very beneficial to enhancing surveillance, monitoring human activities, and information exploitation.

During the course of this project, we have performed experiments and theoretical analysis of the objectives and tasks of the project. We have investigated polarimetric multidimensional imaging in degraded environments. The polarization state of light contains optical and physical properties of the scene. Compared with conventional imaging, polarimetric imaging can reveal additional information about the scene, and it has the potential for material inspection and classification in various applications.

We have investigated deep convolutional neural network model [1-5] using physics based training with three-dimensional (3D) imaging to recognize polarimetric 3D objects in degraded environments such as low light and partial occlusions [2]. We have performed investigation of passive three-dimensional (3D) polarimetric integral imaging [6-8] to extract the 3D polarimetric information of objects in degraded environment, including photon starved conditions and the presence of occlusions. To implement the multi-dimensional imaging system, we have used a low noise visible range camera, and for comparison a long wave infrared (LWIR) range camera. The performance between the two sensors is compared. In addition to lower cost and better compactness, visible range imagers provide much better lateral resolution compared with LWIR imagers.

Multidimensional integral imaging (InIm) using dedicated reconstruction algorithms is effective in challenging degraded environments, wherein 3D images are reconstructed using multiple perspectives of 2D elemental images of the scene. Multidimensional integral imaging improves the signal-to-noise ratio in low light environments due to being optimal in the maximum likelihood sense for read noise dominant images.

Passive polarimetric object recognition is of great interest in the field of imaging because of its ability to enhance the contrast and discriminate the man-made objects from background clutter. However, polarimetric imaging can become challenging in degraded environments such as low light illumination conditions or in partial occlusion. Polarimetric imaging [9-10] is useful for object recognition and material classification because of its ability to discriminate objects based

DISTRIBUTION A: Distribution approved for public release.

on polarimetric signatures of materials. Polarimetric imaging of an object captures important physical properties such as shape and surface properties and can be effective even in low light environments. Integral imaging [11-25, 28-31] is a passive three-dimensional (3D) imaging approach that takes advantage of multiple 2D imaging perspectives to perform 3D reconstruction.

We have investigated a unified polarimetric detection and classification of objects in degraded environments such as low light and the presence of occlusion. This task is accomplished using a deep learning model for 3D polarimetric integral imaging data captured in the visible spectral domain. The neural network system is designed and trained for 3D object detection and classification using polarimetric integral images. We compare the detection and classification results between polarimetric and non-polarimetric 2D and 3D imaging. The system performance in degraded environmental conditions is evaluated using average Miss Rate, average Precision, and F-1 score. The results indicate that for the experiments we have performed, polarimetric 3D integral imaging outperforms 2D polarimetric imaging as well as non-polarimetric 2D and 3D imaging for object recognition in adverse conditions such as low light and occlusions. To the best of our knowledge, this was the first report for polarimetric 3D object visualization and recognition in low light environments and occlusions using a deep learning-based integral imaging. The proposed approach is attractive because low light polarimetric object visualization and recognition in the visible spectral band benefits from much higher spatial resolution, more compact optics, and lower system cost compared with long wave infrared imaging which is the conventional imaging approach for low light environments. Stokes polarization parameters and degree of polarization (DoP) are calculated to extract the polarimetric information of the multidimensional scene. Our experimental evidence showed that low noise visible range camera may outperform the LWIR camera in detection of polarimetric objects under low illumination and other degraded environmental conditions.

Thus, the most significant outcome of our investigation is that multidimensional imaging in visible range may outperform its LWIR imaging counterpart in degraded environments such as low light levels. This holds true for polarimetric as well as non-polarimetric imaging, for visualization as well as in object detection under low illumination and other degraded environmental conditions.

This Final Report does not present all the technical and educational activities and relevant details performed in the entire project due to space considerations. However, the publications reported here contain additional details and coverage of the activities in this project.

Summary of Technical Accomplishments

We have investigated multidimensional object recognition in low light environments and under partial occlusions using deep learning with passive polarimetric integral imaging. We have investigated passive 3D polarimetric integral imaging for target visualization, detection and recognition in low light illumination conditions and partial occlusions using deep learning-based model. We have shown by optical experiments that 3D polarimetric integral imaging using deep

neural networks can be used to improve the target visualization, detection and classification results in low light environment and under partial occlusion. In the experiments, we have employed the Deep Learning neural network [27]. Furthermore, we have compared the performance of the neural network for polarimetric and non-polarimetric integral imaging as well as the system performance with polarimetric 2D imaging. The system performance in degraded environmental conditions is evaluated using average Miss Rate, F-1 score, and average Precision. Our experiments show that for the experiments we have performed, polarimetric integral imaging using deep NN improves the accuracy of target visualization and recognition in low light environment and occlusion. Also, the performance of the 3D polarimetric integral imaging target visualization and recognition is better than polarimetric 2D imaging and non-polarimetric 2D and non-polarimetric 3D target recognition. The proposed approach is attractive because low light polarimetric target recognition in the visible spectral band provides higher spatial resolution, more compact optics, and a lower system cost compared to long wave infrared (LWIR) target recognition system. Relevant experiments have shown that visible range 3D integral imaging may outperform its LWIR counterparts in 2D and 3D.

Thus, the most significant outcome of our investigation is that multidimensional imaging in visible range may outperform its LWIR imaging counterpart in degraded environments such as low light levels. This holds true for polarimetric as well as non-polarimetric imaging, for visualization as well as in object detection under low illumination and other degraded environmental conditions.

1. Polarimetric Sensing: A Review

Polarization is a property of light wave that specifies the geometric orientation of the field oscillations. When an unpolarized light wave is reflected from an object surface, most of the reflected light becomes partially polarized [9-10]. The reflected partially polarized light is captured by recording a set of polarimetric images with multiple polarization directions. The Stokes parameters are calculated using the set of recorded polarimetric images with multiple polarization directions. The Stokes parameters are as following and used to calculate the degree of polarization:

$$\begin{aligned} S_0 &= I^{0^\circ} + I^{90^\circ} \\ S_1 &= I^{0^\circ} - I^{90^\circ} \\ S_2 &= I^{45^\circ} - I^{135^\circ} \\ S_3 &= I^{45^\circ,\pi/2} - I^{135^\circ,\pi/2}, \end{aligned} \tag{1}$$

where S_i ($i=0,1,2,3$) denotes the Stokes parameter, I^{θ} is the intensity of polarized light recorded when the linear polarizer in front of the imaging sensor is placed at an angle of θ with respect to the y-axis, and $I^{\theta,\,\pi/2}$ is the intensity recorded after inserting the quarter wave plate (QWP) in addition to the linear polarizer. The degree of linear polarization (DoLP) is calculated as:

$$\text{DoLP} = \frac{\sqrt{S_1^2 + S_2^2}}{S_0} \tag{2}$$

The DoLP indicates the quantity of polarized light in a wave and its value ranges from 0 to 1. For totally polarized light, the value of DoLP becomes one, and it is zero for unpolarized light. Circular component of polarized light S_3 is very small and rarely measurable in case of passive polarization. As such, in this experiment, the value of S_3 is taken to be negligible.

2. Methodology

2.1 Integral imaging

Integral imaging is a passive three-dimensional (3D) imaging technique which records the intensity as a function of the scene perspectives using a camera array, lenslet array or a single moving camera [12-22]. The unique perspectives of the scene recorded by each camera are known as the elemental images. Some of the advantages of using 3D integral imaging are that it uses parallax and depth reconstructed 3D images to reduce the effects of partial occlusion in front of the scene and to segment out objects of interest from the background. Moreover, 3D reconstructed image has better signal to noise (SNR) as compared to the 2D image in low light environment [24].

A synthetic aperture integral imaging (SAII) system that consists of a single camera on a moving translational stage as shown in Fig. 1(a) is used to capture the polarimetric integral images of the scene. A linear polarizer in front of camera sensor is used to record a set of four images [I^{0°, I^{45°, I^{90°, I^{135°] by rotating the polarizer at angle θ (0°, 45°, 90°, 135°) with respect to y-axis, respectively as shown in Fig. 1(a). Figure 1(b) depicts the pickup process of integral imaging. Once the elemental images are recorded by the moving camera, the scene can be reconstructed by SAII algorithm as shown in Fig. 1(c). The reconstruction of the 3D scene is done by back-propagating the captured elemental images through a virtual pinhole array to a particular depth.

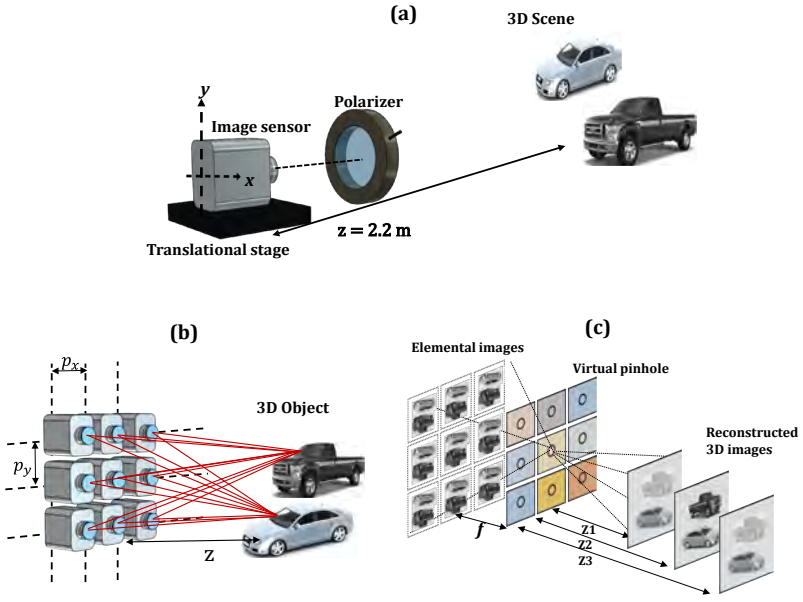

Fig.1. *(a) The principle of polarimetric imaging, (b) synthetic aperture integral imaging (SAII) pickup, and (c) reconstruction stages.*

The polarimetric 3D integral imaging is reconstructed at a particular reconstructed depth z as follow [23]:

$$I_z^{\theta}(x,y)=\frac{1}{O(x,y)}\sum_{m=0}^{M-1}\sum_{n=0}^{N-1}\left[I_{m,n}^{\theta}\left(x-\frac{m\times L_x\times p_x}{c_x\times z/f},y-\frac{n\times L_y\times p_y}{c_y\times z/f}\right)+\varepsilon\right], \quad (3)$$

where (x, y) is the pixel index, $O(x, y)$ is the overlapping pixel number on (x, y), and M and N are the total numbers of polarimetric elemental images in the x and y direction, respectively. In Eq. (3), $I^{\theta}_{m,n}$ is the set of polarimetric elemental images with multiple directions θ [0°, 45°, 90°, 135°] while the subscripts m, n represent the location of the elemental image, and p_x and p_y are the camera pitch size in horizontal (H) and vertical (V) directions, respectively. L_x and L_y are the total number of pixels in each column and row of images, $c_x \times c_y$ is the sensor size of the camera. z/f is the magnification of the camera, z is the reconstruction depth, f is the focal length of camera lens, and ε is the additive camera noise. In this work, we have assumed that the object distances to be known a priori for precise comparison between 2D and 3D imaging to illustrate the proposed object classification method. Object locations were predetermined by measuring the object distance from the sensor using a laser range meter. However, this is not necessary for general applications as the object range can be determined in integral imaging using a variety of approaches [28-31] which determine the plane (z) which gives the best focus for each object in the 3D scene. In our experiments, the 3D images were reconstructed computationally based on the back-projection technique using SAII in Eq. (3). In this experiment, we used two slices of 3D reconstruction at depth z_1 (first polarimetric object depth) and at depth z_2 (second polarimetric object depth).

We used a fully convolution neural network detection model that determines the bounding boxes of the objects present in the image and classifies them simultaneously [32]. It uses an architecture similar to GoogleNet [33] with 24 convolutional layers and 2 fully connected layers. In this network, the input image is divided into an S×S cell grid. Each grid cell predicts B bounding boxes, the confidence score associated with those bounding boxes, and the class probabilities. Each bounding box has five prediction parameters [x, y, w, h, c], where (x, y) coordinate represents the central location of an object inside the box, and (w, h) represents the height and width of a bounding box. The probability of containing the target is represented by the confidence score (c). The intersection over union (IOU) is used to measure the accuracy of the object detector which defines the correlation between the ground truth and the prediction. The confidence score $\Pr(\text{Object})\times \text{IOU}_{\text{pred}}^{\text{truth}}$ becomes zero when there is no object present in the cell. Besides, each cell also predicts the conditional class probability that represents the possibility of whether each class of object is present. The product of conditional class probability and confidence score of individual box provides the class-specific confidence scores for each box and is calculated by Eq. (4) below. These scores contain both the probability of class and the coordinates of bounding boxes of an object, which determine the object detection results [32].

$$\Pr(\text{Class}_i \mid \text{Object})\times \Pr(\text{Object})\times \text{IOU}_{\text{pred}}^{\text{truth}} = \Pr(\text{class}_i)\times \text{IOU}_{\text{pred}}^{\text{truth}} \quad (4)$$

DISTRIBUTION A: Distribution approved for public release.

YOLOv2 neural network used in this project and report offers improved capabilities as compared to the original YOLOv1 such as batch normalization, high-resolution classification, etc. [27]. The batch normalization achieves improved convergence and improvement in the mean average precision (MAP). YOLOv2 uses the concept of anchor boxes that make it possible for the YOLOv2 algorithm to detect multiple objects centered in one grid cell. For evaluating the YOLOv2 neural network, a grid cell size of 7 (S=7) was used. The detection flowchart of YOLOv2 is shown in Fig. 2.

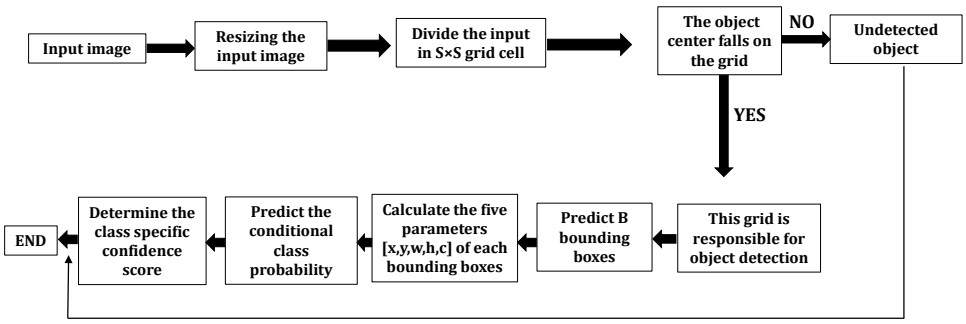

Fig. 2. *Flowchart of deep learning-based neural networks model (YOLOv2).*

2.2 Evaluation Metrics

The prediction is considered as correct if the intersection over union (IOU) exceeds the threshold for the bounding box. IOU is used to measure the overlapping ratio between the detected box and the ground truth box. IOU varies between 0 (no overlap) and 1 (total overlap). The threshold value of IOU in our experiment was set to 0.5. Precision, recall, miss rate, and F1-score are calculated to evaluate the performance of YOLOv2 neural network for object detection and recognition in degraded environments including low light and occluded targets using polarimetric imaging. Precision and recall are defined as *Precision = TP/(TP+FP),* and *Recall = TP/(TP+FN)*, where *TP* is the number of true positives, *FP* is the number of false positives and *FN* is the number of false negatives. Average precision (AP) provides the accuracy of detection as a ratio of correctly predicted observations to the total number of observations and it is calculated as the area under the precision-recall curve. The value of average precision is between 0 to 1. The miss rate represents the true class objects that are not detected. The accuracy of network system is inversely proportional to average miss rate (AM), that is, the lower the average miss rate the higher the precision of the detector. The F1-score in term of precision and recall is defined as,

$$\mathrm{F1} = 2 \times \frac{\mathrm{Precison} \times \mathrm{Recall}}{\mathrm{Precison} + \mathrm{Recall}}. \tag{5}$$

The value of F1-score ranges from 0 to 1.

3. Results and discussion

DISTRIBUTION A: Distribution approved for public release.

A synthetic aperture integral imaging (SAII) experiment was conducted by recording 9 elemental images 3(H)×3(V) with a pitch size of 50 mm in both horizontal (H) and vertical (V) direction using an sCMOS camera (Hamamatsu C11440-42U). The sensor size of camera is 2048(H)×2048(V) with pixel size 6.5μm×6.5μm. The focal length of camera was 50 mm and the exposure time was set to 50 ms. The captured elemental images are processed using SAII algorithm Eq. (3) to reconstruct the 3D image at reconstruction depth *z*. The 2D image used in the experiments is the central image (#5) of 9 (3×3) elemental images. Figure 3 (a), Fig. 3(e) and Fig.3(i) show the central perspective of elemental 2D images in high, low illuminations and low illuminations under occlusion, respectively. Figures 3(c-d), 3(g-h) and 3(k-l) are the non-polarimetric 3D integral images of target at reconstruction depth of z = 1.8m for car and z = 2.2m for truck in high illumination, low illumination and low illumination under occlusion respectively. The advantages of using 3D integral imaging over only averaging the 2D elemental images are that integral imaging uses both angular and intensity information and provides depth reconstructed 3D images which reduce the effects of partial occlusion in front of the scene and to segment out objects of interest from the background [see Fig. 3 (k-l)].

Simple averaging of 9 elemental 2D images is not able to reduce the effect of partial occlusion in front of the scene and to segment out objects of interest from the background [see Fig. 3 (j)]. Figure 3(b), 3(f) and 3(j) show the averaging of 9 elemental 2D images in high illumination, low illumination and low illuminations under occlusion, respectively. Moreover, the 3D reconstruction at a given depth produces the maximum likelihood estimate of the image intensity at the corresponding reconstructed depth [24]. For quantitative comparison of 3D reconstructed integral image and averaging of 9 elemental 2D images, the signal-to-noise ratio (SNR) is measured. The SNR is defined as $\mathrm{SNR} = (\mu_s - \mu_b)/\sqrt{\sigma_s^2 + \sigma_b^2}$ where the mean of the object (signal) is μ_s, and the mean of the background is μ_b. σ_s^2 and σ_b^2 are the variances of object and background areas, respectively. For fair comparison of the integral imaging and averaging of 9 elemental 2D images, the same image regions were considered from objects (signal) and background from the integral 3D image and averaging of 9 elemental 2D images. From the results shown in Table 1, the SNR of 3D integral image outperforms that of averaging of 9 elemental 2D images in low light illumination conditions in both cases (car and truck).

DISTRIBUTION A: Distribution approved for public release.

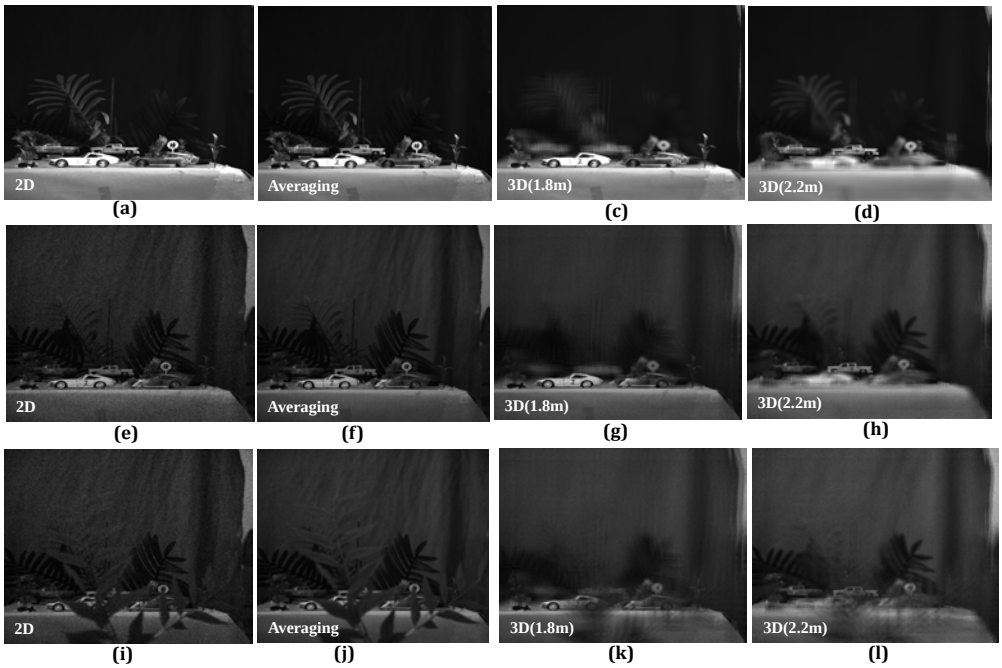

Fig. 3. *(a-d) Integral imaging and averaging of 9 elemental images in high illumination. (a) 2D image (central elemental image) of the scene, (b) averaging of 9 elemental 2D images, (c) 3D reconstructed image focused at z = 1.8m and (d) 3D reconstructed image focused at z = 2.2m. (e-h) Integral imaging and averaging of 9 elemental 2D images in low illumination. (e) 2D image (central elemental image) of the scene, (f) averaging of 9 elemental 2D images, (g) 3D reconstructed image focused at z = 1.8m and (h) 3D reconstructed image focused at z = 2.2m. (i-l) Integral imaging and averaging of 9 elemental 2D images in low illumination under occlusion. (i) 2D image (central image) of the scene, (j) averaging of 9 elemental 2D images, (k) 3D reconstructed image focused at z = 1.8m and (l) 3D reconstructed image focused at z = 2.2m.*

Table 1. SNR Comparison of 3D integral image and averaging of 9 elemental 2D images in low light illumination conditions.

	Car			Truck		
	Central elemental 2D image	Averaging of 9 elemental images	Integral 3D image	Central elemental 2D image	Averaging of 9 elemental 2D images	Integral 3D image
SNR	1.04	1.12	1.26	0.55	0.57	0.83

The captured polarimetric images [I^{0°, I^{45°, I^{90°, I^{135°] with multiple orientations of polarization (0°, 45°, 90°, 135°) are used to calculate the Stokes parameters, and DoLP images using Eq. (1) and Eq. (2), respectively. The polarimetric data set is recorded using integral imaging with various backgrounds to diversify the training set and to provide non training background scenes for testing. Passive polarimetric training data was recorded in high illumination conditions as shown in Fig. 4(a-c). Sixty different scenes were recorded for training the neural network system. Figure 4(a) is

the polarimetric 2D image. Figure 4 (b-c) are the polarimetric 3D images reconstructed at z = 1.9m, and z = 2.3m respectively, in high illumination. Furthermore, to improve the performance of neural network model, data augmentation is used to improve the generalization capabilities of the trained neural network model. This is done by different augmentation techniques which include flipping and adding Gaussian noise with mean 0 and variances of 0.01 and 0.015. Thus, in total, 240 images were generated after data augmentation, which were used for training the model. We have used Adam optimizer with a learning rate of 10^{-3}, batch size of 12, and the network was trained for 400 epochs.

For testing the performance of YOLOv2 training model, passive polarimetric images recorded in low light illumination conditions under occlusion have been used. The noise present in the images due to low light environments is enhanced during the DoLP calculation due to the nonlinear combination of the Stokes parameters. The noise in the 2D image becomes saturated during 2D DoLP calculation in photon-starved conditions as shown in Fig. 4 (d). The 3D DoLP image reduces the noise and mitigates the saturation effect as shown in Fig. 4(e-f). Finally, a total variation denoising is applied to reduce the noise in polarimetric 2D DoLP and 3D DoLP images. The TV denoising algorithm is applied to the set of four 2D images [I^{0^o} , I^{45^o} , I^{90^o} , I^{135^o}] in case of 2D DoLP image, and to the set of four 3D reconstructed images [$I^{0^o}{}_z$, $I^{45^o}{}_z$, $I^{90^o}{}_z$, $I^{135^o}{}_z$] in case of 3D DoLP images. Figure 4 (g-i) show the results of DoLP images after applying the TV denoising. Figure 4 (g) shows the 2D DoLP image after TV denoising and Fig. 4 (h-i) show the 3D reconstructed DoLP images at depth z = 1.9m and 2.3m, respectively after TV denoising.

To ensure the diversity of the testing sample the polarimetric images were recorded in different low light levels and various background scenes. The different low light illumination conditions are estimated in terms of photons per pixel, which ranges from 1.5 to 10 photons per pixel [34]. The polarimetric 2D and reconstructed 3D DoLP images in low light conditions under occlusion after using TV denoising are shown in Fig. 4(g-i). The noisy occluded 2D DoLP image in low light is shown in Fig. 4(g). Figure 4(h-i) show the reconstructed 3D DoLP images at depth z = 1.9 m, and z = 2.3 m, respectively. For testing the neural network system, the total number of polarimetric images in the adverse conditions of low light and under occlusion is 80.

DISTRIBUTION A: Distribution approved for public release.

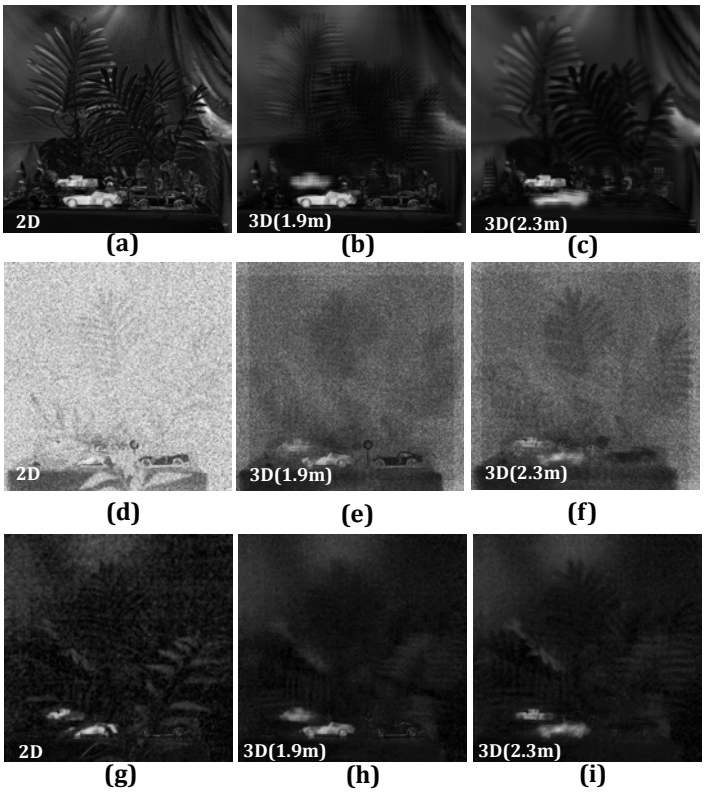

Fig. 4. *(a-c) Polarimetric images in high illumination for training the neural network system. (a) 2D DoLP image of the objects in high illumination, (b) 3D DoLP image reconstructed at z = 1.9m, and (c) 3D DoLP image reconstructed at z =2.3m. (d-f) Polarimetric images in low light illumination and occlusion without TV denoising. (d) 2D DoLP image of the objects, (e) 3D DoLP image reconstructed at z = 1.9 m, and (f) 3D DoLP image reconstructed at z = 2.3 m. (g-i) Polarimetric images in low light illumination and occlusion after TV denoising. (g) 2D DoLP image of the objects, (h) 3D DoLP image reconstructed at z = 1.9 m, and (i) 3D DoLP image reconstructed at z = 2.3 m. The estimated photons/pixel in low illumination conditions is 2.1.*

The YOLOv2 neural network is used to detect and classify the objects in polarimetric imaging. The detection and classification results of 2D and 3D polarimetric images obtained after training the YOLOv2 network are shown in Figures (5) and (6), respectively. It can be noticed that the success rate of detection and classification of both polarimetric objects (car and truck) is not guaranteed in the case of 2D polarimetric images due to occlusion and low light levels as shown in Fig. (5). In our experiments, for 2D polarimetric images in degraded environment, the model fails to detect and classify the polarimetric objects correctly in most of the cases. The effects of low light (low photons per pixel) and occlusion reduce the classification accuracy of the neural network, and increase false detection rate and miss rate. Fig. 5 (a-d) shows that while both car and truck are present in the scene, only car is detected correctly. The classification results for the 2D imaging worsen as we lower the illumination levels. For example, both the car and truck are

DISTRIBUTION A: Distribution approved for public release.

classified as truck in Fig. 5 (e-f). However, 3D integral imaging reduces the effects of occlusion and low light to improve classification with the polarimetric objects. The successful detection and classification of both polarimetric objects in different low light levels and occlusion with 3D polarimetric images is shown in Fig. 6.

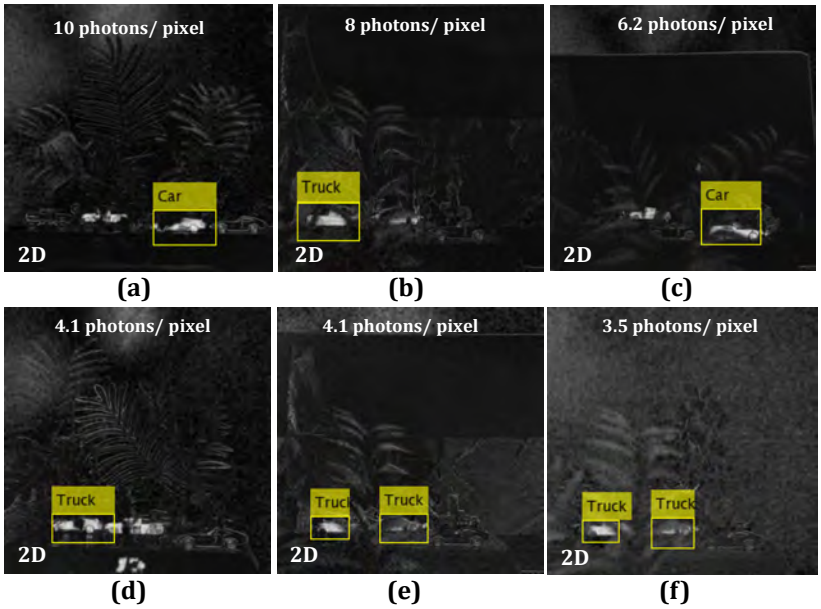

Fig. 5. *2D polarimetric object classification is not successful in the experiments with degraded environment. Detection and classification results of YOLOv2 network system under different light conditions and occlusion for 2D polarimetric images. The estimated photons per pixel of 2D DoLP images are (a) 10 photons/pixel, (b) 8 photons/pixel, (c) 6.2 photons/pixel, (d) 4.1 photons/pixel, (e) 4.1 photons/pixel, and (f) 3.5 photons/pixel.*

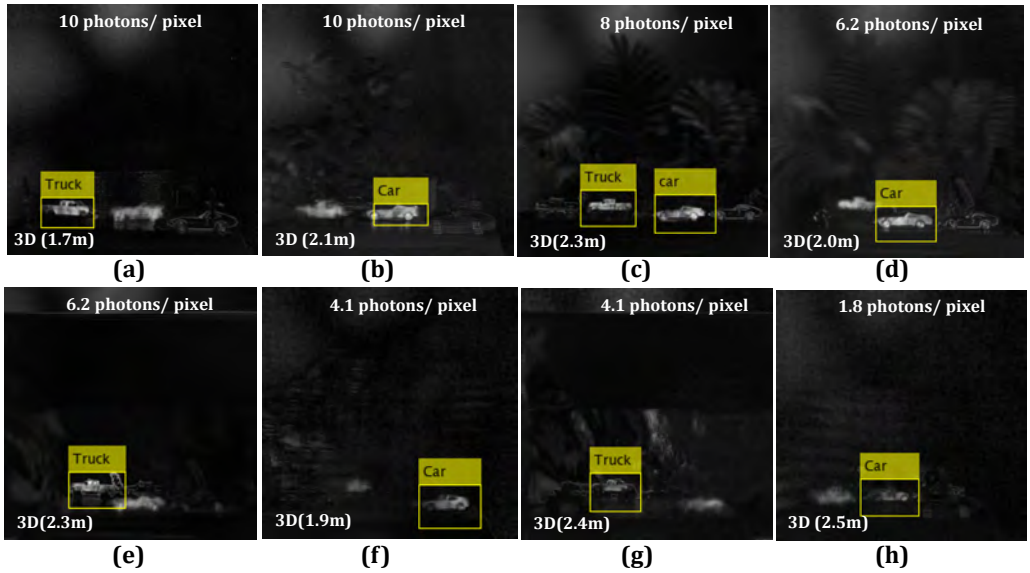

DISTRIBUTION A: Distribution approved for public release.

Fig. 6. *Successful detection and classification result of YOLOv2 network system under different low light conditions and occlusion for 3D polarimetric images. The estimated photons per pixel of 3D DoLP image are (a) 10 photons/pixel at z = 1.7m, (b) 10 photons/pixel at z = 2.1m (c) 8 photons/pixel at z = 2.3m, (d) 6.2 photons/pixel at z = 2.0m, (e) 6.2 photons/pixel at z = 2.3m, (f) 4.1 photons/pixel at z = 1.9m, (g) 4.1 photons/pixel at z = 2.4m, and (h) 1.8 photons/pixel at z = 2.5m.*

For performance evaluation of the presented model for polarimetric and non-polarimetric imaging, average precision (AP), average miss rate (AM), and F1-score are calculated. Table 2 presents the results of the YOLOv2 neural network for objects detection and classification in polarimetric and non-polarimetric imaging. In our experiments, it was difficult to detect and classify objects in low light conditions and occlusion using 2D polarimetric imaging, and non-polarimetric 2D and 3D imaging. Under these circumstances, the detection and classification accuracy of YOLOv2 neural network suffered adversely. As shown in Table 2, the network failed to reliably detect and classify objects in 2D polarimetric imaging, and non-polarimetric 2D and 3D imaging in low light illumination and occlusion.

Table 2. Classification performance comparison of YOLOv2 neural network for polarimetric and non-polarimetric imaging dataset in low light and occlusion of targets.

	Polarimetric image detection				**Non-polarimetric image detection**			
	3D image		**2D image**		**3D image**		**2D image**	
	Truck	Car	Truck	Car	Truck	Car	Truck	Car
Average Precision	0.64	0.57	0.11	0.10	0.10	0.25	0.08	0.09
Average Miss rate	0.38	0.45	0.87	0.88	0.96	0.92	0.98	0.96
F1-score	0.52	0.46	0.21	0.16	0.11	0.12	0.08	0.10

Furthermore, quantitative analysis of classification accuracy of neural network for different light conditions and in the presence of occlusion are presented. The polarimetric dataset in low light illumination and occlusion are equally divided in their respective low light illumination conditions, that is, from 1.5 photons/pixel to 10 photons/pixel. The F1-score for polarimetric datasets in different low light illumination conditions are evaluated. In Appendix A, Figure 2A shows the graph of F1-score of neural network with respect to light levels (photons/pixel) for 2D and 3D polarimetric images. The quantitative analysis indicates that in our experiments the 3D polarimetric images enabled the neural network to detect and classify the targets effectively in the range of 6-10 photons/pixel. However, the neural network system failed to reliably detect and classify the 2D polarimetric images at all low light levels. Future works include investigation of various types of integral imaging architectures and algorithms [35-36].

DISTRIBUTION A: Distribution approved for public release.

4. Statistical Approach to Extract 3D polarimetric information in Low Light Levels

We propose a statistical approach to extract 3D polarimetric information from DoP in low illumination. The derived 3D Stokes parameters which indicate the intensity differences between orthogonal images are read-noise-dominated with a zero mean Gaussian distribution, [$N(0, \sigma^2)$]. However, the 3D image intensities from in-focus areas of a polarimetric material are dependent on the orientation of the polarimetric optical components. The corresponding Stokes parameters will be a non-zero mean Gaussian distribution, [$N(\mu, \sigma^2)$, $\mu \neq 0$]. The Chi distribution is the square root of the sum of squares of a set of independent random variables where each follows a standard normal distribution. Thus, we can distinguish the 3D polarimetric properties in the scene by analyzing the probability distribution of the numerator of DoP with each Stokes parameter normalized by its standard deviation:

$$X_z = \sqrt{\sum_{i=1}^{3} \left(S_i^z/\sigma_i\right)^2}, X_z \sim Chi\ distribution, if\ S_i^z \sim N\left(0, \sigma_i^2\right). \quad (6)$$

The 3D Stokes Parameters Si, i = [1, 2, 3] are a formed by subtraction of two orthogonal 3D polarimetric images. A 3D polarimetric InIm experiment was performed in low light environment. A digital camera, Hamamatsu C11440-42U, with a Scientific CMOS (SCMOS) image sensor FL-400 was used for SAII. The image sensor has 2048 (H) × 2048 (V) pixels, with a pixel size of 6.5 (H) × 6.5 (V) μm. The exposure time was set as 10 ms. Focal length of the camera was 50 mm. In the experiment, a mannequin with an attached piece of linear polarizer film on its left chest was placed approximately 3.2 meters from the camera, and the background was approximately 5.2 meters away. SAII was preformed using a moving camera with a total of 49 [7(H)×7(V)] perspectives. The pitch between adjacent perspectives was 30 mm in both the horizontal and vertical directions. As circularly polarized light rarely occurs in nature and the material used in the scene has only linear polarization properties, the Stokes parameter (S3) corresponding to circular polarization should be 0.

The captured 2D images and 3D reconstructed images using conventional InIm under low illumination are shown in Fig. 7a (i) and Fig. 7a (ii-iii), respectively. An example of the generated 2D image (ξ) without Noffset is shown in Fig. 7b(i). In addition, this image can be used to estimate the number of photons arriving on the image sensor. The gray scale intensity of the image is first converted to electrons by the conversion factor of the sensor. The number of photons for each pixel is then derived by dividing the converted electrons with the sensor's quantum efficiency: $\gamma = \xi \times CF/QE$, where γ is the estimated number of photons, CF = 0.46 electrons/count is the conversion factor, and QE = 70% is quantum efficiency. In Fig. 7b(i), an average of 2.13 photons/pixel are estimated in low illumination condition. Figures 7 b(ii) and b (iii) illustrate the 3D images at 3.2 m and 5.2 m, respectively. Image SNR is used to compare the 2D and 3D image qualities. Our proposed approach improves the SNR by 7 times.

DISTRIBUTION A: Distribution approved for public release.

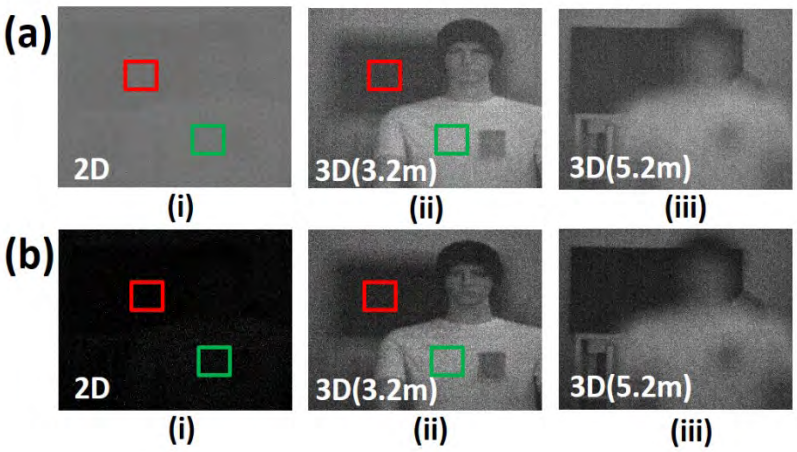

Fig. 7. Conventional InIm in low light. (a) Images with camera offset (N_{offset}). (b) Images without N_{offset}. (i) Sample 2D perspective image. (ii) 3D image focused on object plane. (iii) 3D image focused on background. Green and red windows correspond to object and background areas for calculation of SNR. SNR=4.9 for passive 3D imaging. SNR=0.7 for passive 2D. Estimated photons/pixel = 2.13.

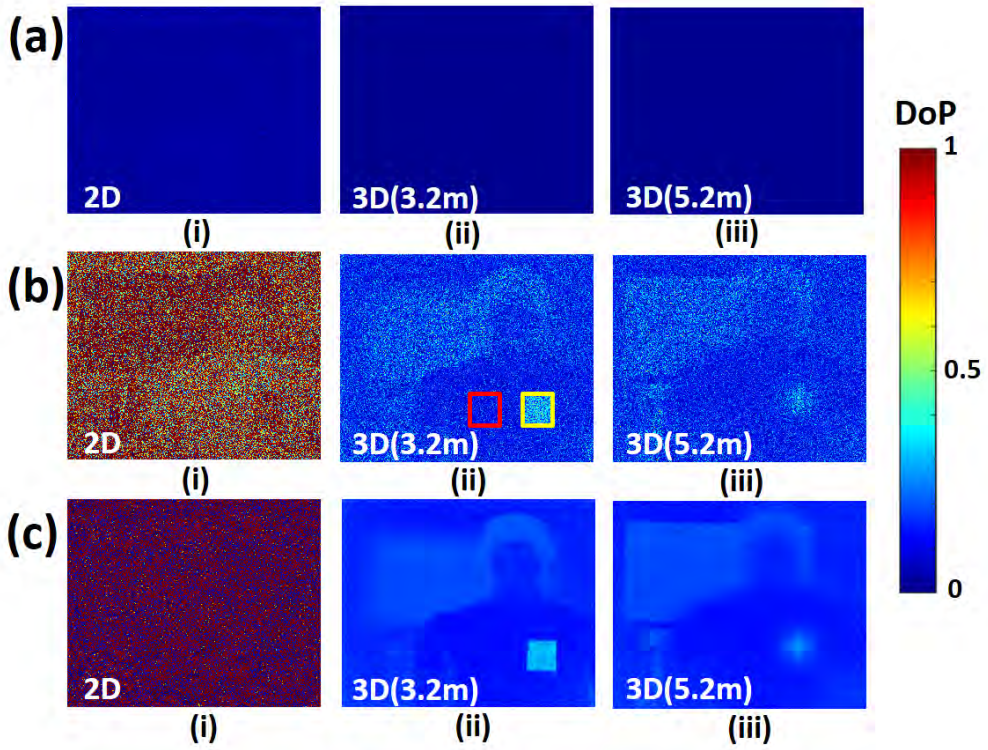

Fig. 8. 2D and 3D DoP images. (a) with camera offset (N_{offset}), (b) without N_{offset}, and (c) without N_{offset} and by applying total variation algorithm. (i) 2D DoP. (ii) 3D DoP at z = 3.2 m. (iii) 3D DoP at z = 5.2m. Yellow and red windows correspond to the polarimetric and non-polarimetric material areas. Estimated photons/pixel = 2.13.

Fig. 8 shows the experimental results of the calculated DoP images between the proposed approach and conventional 2D methods. The reconstructed objects in both depths (3.2 m and 5.2 m) are sharpened while the edges are preserved. The 2D DoP with TV [Fig. 8c(i)] cannot provide the correct polarimetric information, which illustrates the advantage of the proposed 3D polarimetric approach.

We apply Kullback-Leibler Divergence to measure the relative entropy of probability distributions of 3D DoP (Xz) between signal and noise, along the reconstruction depth range (z) to illustrate the reduction in noise using our polarimetric approach. The signal is defined to be the polarimetric material area, and noise is for non-polarimetric material. Figure 9(a)-(b) illustrates the histograms of the random variables derived from the 3D DoP numerator at 3.2 m and 5.2 m, respectively. The windows were selected in areas of polarimetric material (PM), and non-polarimetric material (NPM) of the scene. Fig. 9(c) depicts the KL Divergence between the PM and NPM areas along the depth range (Z). At focused depth position of ~3.2 m, the random variable probability distribution in the PM area will not follow a Chi distribution, which is different with the NPM area, and the KL divergence reaches a maximum. When the PM is out-of-focus, the corresponding Xz ~ Chi distributed and the KL Divergence approaches 0. Note that we cannot extract 3D

polarimetric information from conventional 2D polarimetric imaging in low light conditions. We have performed experimental results for 3D polarimetric imaging under low illumination with an estimated 2.13 photons per pixel captured by the camera. In very low illumination (photons/pixel < 20), the calculated 3D DoP decreases sharply with large standard deviation because of low SNR and measurement uncertainty due to noise. However, our approach substantially outperforms 2D imaging in terms of extracting depth and polarimetric information.

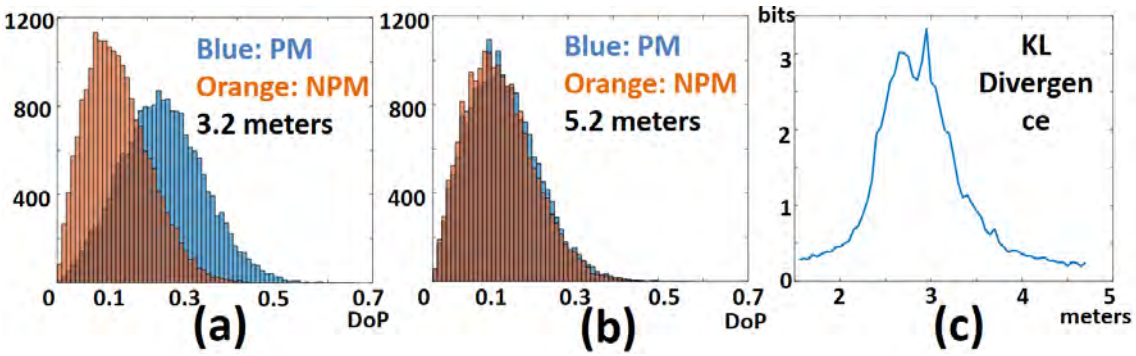

Fig. 9. Histograms of 3D DoP *numerator [Eq. 5] at (a) 3.2 m focused on object, and (b) 5.2 m (background). PM = polarimetric material, NPM = non-polarimetric material. Estimated photons/pixel = 2.13. Windows [Fig. 3b(ii)] were selected on areas corresponding to the PM area (yellow box), and NPM area (red box). (c) Kullback-Leibler Divergence between the windows along depth range* Z.

5. Conclusions

In this project, we have theoretically and experimentally investigated passive multidimensional object visualization, detection and classification using passive 3D polarimetric integral imaging in the presence of environmental degradations including low light levels and partial occlusion of the scene. We have used a variety of analytical tools including statistical approaches and deep learning neural networks for the analysis. We have examined both visible range imaging and imaging using long wave IR (LWIR) sensors. The performance of the proposed 3D polarimetric imaging model is compared with polarimetric 2D, and non-polarimetric 2D and 3D images for object visualization, detection and recognition. In our experiments with 2D and 3D polarimetric and non-polarimetric imaging, we observed that 3D polarimetric images can effectively detect and classify the polarimetric objects in different low light levels ranging from 1.5 photons per pixel to 10 photons per pixel, and in the presence of occlusions. In our experiments, for both polarimetric 2D imaging and non-polarimetric 2D and 3D imaging, the network failed to reliably detect and classify the object at various low light levels and with occlusion. While these experiments were limited due to the limited scope of this project, they show the potential benefits of 3D polarimetric integral imaging system. Another important observation was that visible range multidimensional integral imaging may outperform LWIR imaging systems for polarimetric imaging. This evidence may lead to substantial benefits for the US Air Force and DoD in general for deploying more compact

and cost effective system using visible range sensors instead of bulkier and more costly LWIR imaging systems.

References

1. D. Erhan, C. Szegedy, A. Toshev, et al, “Scalable object detection using deep neural networks,” IEEE Conference on Computer Vision and Pattern Recognition, 2155-2162(2014).
2. K. Usmani, G. Krishnan, T. O’Connor, and B. Javidi, “Deep learning polarimetric three-dimensional integral imaging object recognition in adverse environmental conditions,” Optics Express, 29 (8), 12215-12228 (April 22, 2021).
3. P. F. Felzenszwalb, R. B. Girshick, D. Mcallester, and D. Ramanan, “Object detection with discriminatively trained part-based models,” IEEE Trans. Pattern Anal. Mach. Intell. **32**(9), 1627, 2010.
4. K. He, X. Zhang, S. Ren, and J. Sun, “Deep Residual Learning for Image Recognition,” IEEE International Conference on Computer Vision, 770-778 (2015).
5. V. Bevilacqua, A. Brunetti, G. D. Cascarano, A. Guerriero, F. Pesce, M. Moschetta, and L. Gesualdo, “A comparison between two semantic deep learning frameworks for the autosomal dominant polycystic kidney disease segmentation based on magnetic resonance images”, BMC Medical Informatics and Decision Making, **19**(9) (2019).
6. A. Carnicer and B. Javidi, “Polarimetric 3D integral imaging in photon starved conditions,” Opt. Express **23**(5), 6408–6417 (2015).
7. X. Shen, A. Carnicer, and B. Javidi, “Three-dimensional polarimetric integral imaging under low illumination conditions,” Opt. Lett. **44**(13), 3230–3233 (2019).
8. K. Usmani, T. O’Connor, X. Shen, P. Marasco, A. Carnicer, D. Dey, and B. Javidi, “ Three-dimensional polarimetric integral imaging in photon-starved conditions: performance comparison between visible and long wave infrared imaging”, Opt. Express **28**(13), 19281–19294 (2020).
9. G.P. Konnen, *Polarized light in nature* (Cambridge University, 1985).
10. M. Born and E. Wolf, *Principles of Optics: Electromagnetic Theory of Propagation, Interference and Diffraction of Light* (Cambridge University, 1999).
11. A. Markman, X. Shen, and B. Javidi, “Three-dimensional object visualization and detection in low light illumination using integral imaging”, Opt. Lett. **42**(16), 3068-3071 (2017).
12. G. Lippmann, “Epreuves reversibles donnant la sensation du relief”, J. Phys. **7**, 821-825 (1908).
13. N. Davies, M. McCormick, and L. Yang, “Three-dimensional imaging systems: a new development,” Appl. Opt. **27**(21), 4520-4528 (1988).
14. H. Arimoto and B. Javidi, "Integral Three-dimensional Imaging with digital reconstruction," Opt. Lett. **26**(3), 157-159 (2001).
15. F. Okano, H. Hoshino, J. Arai, and I. Yuyama, “Real-time pickup method for a three-dimensional image based on integral photography,” Appl. Opt. **36**(7), 1598-1603 (1997).
16. M. Martinez-Corral, A. Dorado, J. C. Barreiro, G. Saavedra, and B. Javidi, “Recent advances in the capture and display of macroscopic and microscopic 3D scenes by integral imaging,” Proc. IEEE **105**(5), 825-836 (2017).
17. A. Stern and B. Javidi, “Three-dimensional image sensing and reconstruction with time-division multiplexed computational integral imaging”, Appl. Opt. **42**(35), 7036-7042 (2003).

DISTRIBUTION A: Distribution approved for public release.

18. E. H. Adelson and J. R. Bergen, “The plenoptic function and the elements of early vision,” Computational Models of Visual Processing **1**, 3-20 (1991).
19. J. Liu, D. Claus, T. Xu, T. Keßner, A. Herkommer, and W. Osten, "Light field endoscopy and its parametric description," Opt. Lett. **42**(9), 1804-1807 (2017).
20. G. Scrofani, J. Sola-Pikabea, A. Llavador, E. Sanchez-Ortiga, J.C. Barreiro, G. Saavedra, J. Garcia-Sucerquia, and M. Martinez-Corral, “FIMic: design for ultimate 3D-integral microscopy of in-vivo biological samples,” Biomed. Opt. Express, **9**(1), 335-346 (2018).
21. J. Arai, E. Nakasu, T. Yamashita, H. Hiura, M. Miura, T. Nakamura, R. Funatsu, “Progress overview of capturing method for integral 3-D imaging displays,” Proc. IEEE **105**(5), 837-849 (2017).
22. M. Yamaguchi, "Full-parallax holographic light-field 3-D displays and interactive 3-D touch," Proc. IEEE **105**(5), 947-959 (2017).
23. J. S. Jang and B. Javidi, “Three-dimensional synthetic aperture integral imaging,” Opt. Lett. **27**(13), 1144–1146 (2002).
24. B. Tavakoli, B. Javidi, and E. Watson, “Three dimensional visualization by photon counting computational integral imaging,” Opt. Express **16**(7), 4426–4436 (2008).
25. S. H. Hong and B. Javidi “Three-Dimensional Visualization of Partially Occluded Objects Using Integral Imaging”, J. Display Technol. **1**(2), 354-359 (2005).
26. L. I. Rudin, S. Osher, and E. Fatemi, “Nonlinear total variation based noise removal algorithms,” Physica D **60**, 259–268 (1992).
27. J. Redmon, A. Farhadi, “YOLO9000: Better, Faster, Stronger”, Proc. IEEE Conf. Comput. Vis. Pattern Recognit. (CVPR), 6517–6525 (2017).
28. M. Daneshpanah and B. Javidi, “Profilometry and optical slicing by passive three dimensional imaging,” Opt. Lett., **34** (7), 1105–1107, (2009).
29. A. Martinez-Uso, P. Carmona, F. Pla, B. Javidi, "Depth estimation in Integral Imaging based on a maximum voting strategy," IEEE J. Display Technol., **12**, 1715-1723 (2016).
30. X. Xiao, B. Javidi, M. Martinez-Corral, and A. Stern, “Advances in three-dimensional integral imaging: sensing, display, and applications,” Appl. Opt., **52**(4), 546–560 (2013).
31. D. Aloni and Y. Yitzhaky, “Automatic 3D object localization and isolation using computational integral imaging,” Appl. Opt., **54**(22), 6717–6724 (2015)
32. J. Redmon, S. Divvala, R. Girshick, A. Farhadi, “You Only Look Once: Unified, Real-Time Object Detection”, Proc. IEEE Conf. Comput. Vis. Pattern Recognit. (CVPR), 779–788 (2016).
33. J. Deng, W. Dong, R. Socher, L. Li, K. Li, and L. Fei-Fei, “ImageNet: A large-scale hierarchical image database,” Proc. IEEE Conf. Comput. Vis. Pattern Recognit. (CVPR), 248–255 (2009).
34. A. Stern, D. Aloni, and B. Javidi, “Experiments with Three-dimensional integral imaging under low light levels,” IEEE Photonics J. 4(4), 1188–1195 (2012).
35. M. Martínez-Corral and B. Javidi, "Fundamentals of 3D imaging and displays: a tutorial on integral imaging, light-field, and plenoptic systems," Adv. Opt. Photon. **10**(3), 512-566 (2018).
36. B. Javidi, F. Pla, J. M. Sotoca, X. Shen, P. Latorre-Carmona, M. Martínez-Corral, R. Fernández-Beltrán, and G. Krishnan, "Fundamentals of automated human gesture recognition using 3D integral imaging: a tutorial," Adv. Opt. Photon. **12**(4), 1237-1299 (2020).

Appendix A

Prof. Bahram Javidi, University of Connecticut; Email: Bahram.Javidi@UConn.edu

This Appendix A presents additional results for the experiments presented in Section 3 and figures 4-6. Figure 1A shows the graph of log average miss rate for 2D and 3D polarimetric test targets (cars and trucks) in the scene under various low light conditions. The evaluation metrics and graph indicate that the performance of the YOLOv2 neural network in case of 3D polarimetric images in the adverse conditions of low light and occlusion has outperformed the 2D polarimetric, and non-polarimetric 2D and 3D imaging. In our experiments, an improvement of 372.7% and 283.33% was achieved in F1 score in case of Truck and Car classification, respectively from 3D non-polarimetric to 3D polarimetric image detection in low light environments under occlusion. An improvement of 147.6% and 187.5% was achieved in F1 score in case of Truck and Car detection, respectively from polarimetric 2D DoLP image to polarimetric 3D DoLP image detection in low light environments under occlusion. Therefore, polarimetric image with 3D integral imaging achieved maximum accuracy in low light illumination condition under occlusion.

Figure 2A shows the graph of F1-score of neural network with respect to light levels (photons/pixel) for 2D and 3D polarimetric images. The quantitative analysis indicates that in our experiments the 3D polarimetric images enabled the neural network to detect and classify the targets effectively in the range of 6-10 photons/pixel. However, the neural network system failed to reliably detect and classify the 2D polarimetric images at all low light levels.

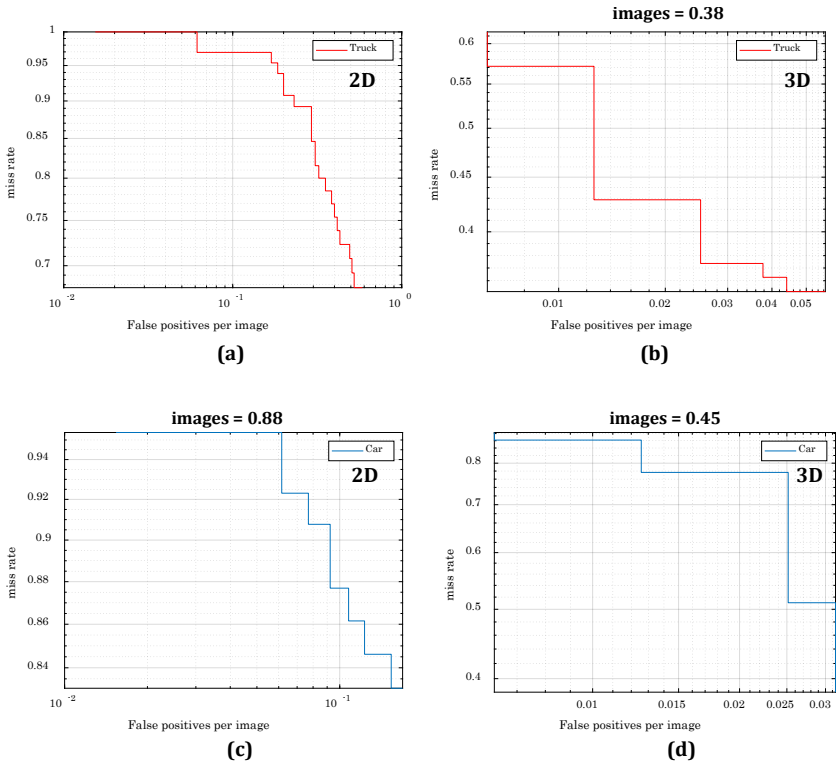

Fig. 1A. *Log average miss rate of deep learning neural network system for polarimetric objects (car and truck) detection and classification in 2D and 3D images. (a) Truck detection in 2D polarimetric images, (b) Truck detection in 3D*

DISTRIBUTION A: Distribution approved for public release.

polarimetric images, (c) Car detection in 2D polarimetric images and (d) Car detection in 3D polarimetric images.

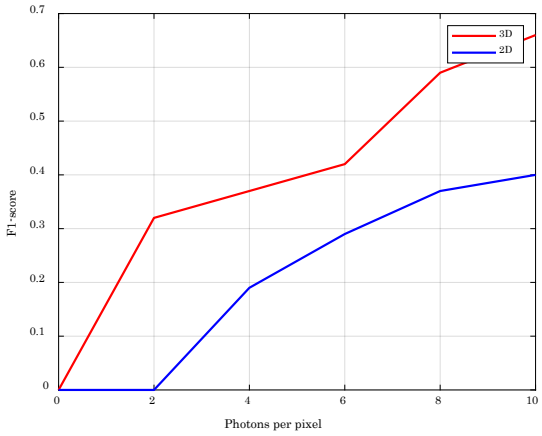

Fig. 2A. *F1 score with different light levels (photons/pixel) for 2D and 3D polarimetric target classification in degraded environment including low light and occlusion.*

Education, Training, Professional Development, and Technical Collaboration:

Student Training

Five PhD graduate students (Kashif Usmani, Timothy O'Connor, Gokul Krishnan, Pranav Wani, Xin Shen) collaborated on this project (see Table 3). One PhD student (Kashif Usmani, MS degree in Applied Physics) is performing experiments on this project and has been working on polarimetric experiments. Gokul Krishnan is a fourth year PhD student with MS degree in electrical engineering and signal processing background who is also assisting with theoretical developments in deep learning neural networks. Another former PhD student (Timothy O'Connor) has graduated and was involved to assist with the experiments. The students are involved in theoretical, experimental, and numerical simulations in this project. The students worked together to build the experimental system, collect data, develop the dedicated algorithms, participate in presentations about the project, write journal and conference papers, etc. The students have attended on-line conferences to further enhance their education and research experience. This is a cross disciplinary project and there is good interaction between researchers with background in electrical engineering, physics, and mathematics/statistics.

Table 3: List of Graduate Students involved in the project, and their status

Name (Graduate Students)	Status, Graduation Date	Current Position

Gokul Krishnan	4th year PhD Student	PhD student at UConn
Timothy O'Connor	Graduated in 2022	Industry
Kashif Usmani	4th year PhD Student	PhD student at UConn
Pranav Wani	3rd year PhD Student	PhD student at UConn
Dr. Xin Shen	Former PhD students, Graduated	Assistant Professor at University of Hartford

Technical and Scientific Collaborations

We continue to collaborate with scientists and engineers at the Sensors Directorate of the Wright Patterson Air Force Base, including Dr. Pete Marasco EO/IR Sensing Technology Adviser. Our objective is to provide the results of our research in collaboration with AFRL colleagues, including field tests, long range applications, and using their particular image sensors of interest.

We have communicated our experimental results with our AFRL colleagues (Dr. Peter Marasco (Peter.Marascro@us.af.mil), EO/IR Sensing Technology Adviser) at the Sensors Directorate of the Wright Patterson Air Force Base. Dr. Marasco, AFRL is interested in polarimetric imaging performed at low light levels in visible spectrum with CMOS imagers. The lateral resolution of the LWIR imagers may be too low for the applications of interest to AFRL. According to Dr. Marasco, the results from this AFOSR project has potential for transition to AFRL.

We have worked with Hamamatsu Photonics CMOS cameras and photon counting EMCCD cameras for low light imaging experiments. The Hamamatsu cameras have been obtained from Hamamatsu Photonics Research Lab at no cost to this AFOSR project. The Hamamatsu scientists have stayed in our Lab to train the students on how to work with the cameras.

We have collaborated with a professor of statistics at UConn (Prof. Dipak Dey) to investigate and apply Bayesian solutions when sensing low light scenes with CMOS image sensors which introduce noise in the detection process at no cost to this AFOSR project. We have also collaborated with a professor of Physics at University of Barcelona, Spain who is following our publications, and is investigate polarimetric imaging at low light levels at no cost to this AFOSR project. We are collaborating with a deep learning neural networks expert who is a professor at University of Jaume I in Castellon, Spain at no cost to this AFOSR project. Other collaborators include my former PhD student, Dr. Inkyu Moon who is currently a professor at DGIST university in South Korea; and my former post doctoral student, Dr. Adrian Stern who is a professor and Head at Ben Gurion University in Israel. These collaborations were at no cost to the AFOSR project.

DISTRIBUTION A: Distribution approved for public release.

Dissemination and Publication of Results, and List of Publications:

The following is a list of publications including journal papers, conference papers and presentations. Our goal was to publish our results in the top journals in the field and premiere conferences in optics and photonics, and present our work in high visibility venues such as Plenary Address, Keynote Address, and Invited Papers to interested communities in optics, photonics, and imaging so that the results can be widely disseminated. In addition, the PI takes advantage of opportunities to present his work in seminars at companies and universities, student chapters, and government Labs. During this report period, during COVID pandemic there were no in person events due to COVID19 circumstances. We apologize in advance if some papers acknowledging the AFOSR sponsor are omitted. A number of papers were Top Downloads of the journals.

Publication Summary:
20 Peer Reviewed Journal Articles
10 Conference Proceedings published

Sample Journal Publications

1. K. Usmani, G. Krishnan, T. O'Connor, and B. Javidi, "Deep learning polarimetric three-dimensional integral imaging object recognition in adverse environmental conditions," Optics Express, 29 (8), 12215-12228 (April 22, 2021).
2. Rakesh Joshi, Gokul Krishnan, Timothy O'Connor, and Bahram Javidi, "Signal detection in turbid water using temporally encoded polarimetric integral imaging," Optics Express, 28, 36033-36045, November 2020.
3. B. Javidi, A. Carnicer, J. Arai, T. Fujii, H. Hua, H. Liao, M. Martínez-corral, F. Pla, A. Stern, L. Waller, Q. H. Wang, G. Wetzstein, M. Yamaguchi, and H. Yamamoto, "Roadmap on 3D integral imaging: sensing, processing, and display," Optics Express, **28**(22), pp. 32266-32293 (October 2020). **Top Download of Optics Express**
4. Vladislav Kravets, Bahram Javidi, and Adrian Stern, "Compressive imaging for defending deep neural networks from adversarial attacks," Optics Letters 46, 1951-1954 (April 2021).
5. T. O'Connor, A. Markman, B. Javidi, "Overview of three-dimensional integral imaging-based object recognition in low illumination conditions with visible range image sensors," SN Applied Sciences, Springer Nature, 2:1724, 2020.
6. Kashif Usmani, Timothy O'Connor, Xin Shen, Pete Marasco, Artur Carnicer, Dipak Dey, and Bahram Javidi, "Three-dimensional polarimetric integral imaging in photon-starved conditions: performance comparison between visible and long wave infrared imaging," Optics Express 28, issue 13, 19281-19294 (June 22, 2020).
7. Gokul Krishnan, Rakesh Joshi, Timothy O'Connor, Filiberto Pla, and Bahram Javidi, "Human Gesture Recognition under Degraded Environments using 3D-Integral Imaging and Deep Learning," Optics Express, 28, #13, 19711-19725 (June 22, 2020). **[Top Download of Optics Express]**

8. Kashif Usmani, Timothy O'Connor, Xin Shen, Pete Marasco, Artur Carnicer, Dipak Dey, and Bahram Javidi, "Three-dimensional polarimetric integral imaging in photon-starved conditions: performance comparison between visible and long wave infrared imaging," Opt. Express 28, issue 13, 19281-19294 (2020).
9. Adam Markman, Timothy O'Connor, Hisaya Hotaka, Shinji Ohsuka, and Bahram Javidi, "Three-dimensional integral imaging in photon starved environments with high sensitivity image sensors," Optics Express, vol. 27, 26355-26368, 2019.
10. Hisaya Hotaka, Timothy O'Connor, Shinji Ohsuka, and Bahram Javidi, "Photon-counting 3D integral imaging with less than a single photon per pixel on average using a statistical model of the EM-CCD camera," Optics Letters, **45**(8), 2327-2330 (2020).
11. Artur Carnicer, Salvador Bosch, and Bahram Javidi, "Mueller Matrix Polarimetry with 3D Integral Imaging," Optics Express, 27, no. 8, pp. 11525-11536 (2019).
12. Xin Shen, Artur Carnicer, and Bahram Javidi, "Three-dimensional polarimetric integral imaging under low illumination conditions," Optics Letters, vol. 44, no. 13, pp. 3230-3233, 2019.
13. Gokul Krishnan, Rakesh Joshi, Timothy O'Connor, Filiberto Pla, and Bahram Javidi, "Human Gesture Recognition under Degraded Environments using 3D-Integral Imaging and Deep Learning," Optics Express, 28, #13, 19711-19725 (2020).
14. Rakesh Joshi, Timothy O'Connor, Xin Shen, Michael Wardlaw, and Bahram Javidi, "Optical 4D signal detection in turbid water by multi-dimensional integral imaging using spatially distributed and temporally encoded multiple light sources," Optics Express, 28, pp. 10477-10490, 2020.
15. 8. K. Ahmadi, P. Lattore Carmona, B. Javidi, and A. Carnicer, "Polarimetric identification of 3D-printed nano particle encoded optical codes," IEEE Photonics Journal, Vol. 12, Number 3, pp. 1-10, 6500810, 2020.
16. Artur Carnicer, Salvador Bosch, and Bahram Javidi, "Mueller Matrix Polarimetry with 3D Integral Imaging," Optics Express, 27, no. 8, pp. 11525-11536 (April 2019).
17. Xin Shen, Artur Carnicer, and Bahram Javidi, "Three-dimensional polarimetric integral imaging under low illumination conditions," Optics Letters, vol. 44, May 3rd, 2019. 05/03/2019
18. Jose M. Sotoca, Pedro Latorre-Carmona, Filiberto Pla, Bahram Javidi, "Depth and all-in-focus image estimation in Synthetic Aperture Integral Imaging under partial occlusions" IEEE Access Journal, Volume 7, Issue 1, Pages 1052-1067, December 2018.

Conference Papers:

19. Kashif Usmani, Gokul Krishnan, Timothy O'Connor, and Bahram Javidi, "Overview of Object Detection in Low Light Using Deep Learning and Polarimetric Three-Dimensional Integral Imaging," Imaging 2022 congress, Sponsored by Optica (OSA), 11-15 July 2022, Vancouver, Canada.

20. Kashif Usmani, Timothy O'Connor, Peter Marasco, Bahram Javidi, “Visible and long-wave infrared imaging in degraded environments using three-dimensional polarimetric integral imaging,” OSA Imaging and Applied Optics Congress, Vancouver, Canada, July 19-22, 2021.
21. Pranav Wani, Kashif Usmani, Gokul Krishnan, Timothy O'Connor, Bahram Javidi, “Object Classification in Photon-Starved Conditions using 3D Integral Imaging: Performance Comparison Between Visible and Longwave Infrared Imaging,” OSA Imaging and Applied Optics Congress, Vancouver, Canada, July 19-22, 2021.
22. Rakesh Joshi, Bahram Javidi, “Overview of integral imaging-based optical signal detection in turbid water using temporally encoded light sources,” OSA Imaging and Applied Optics Congress, Vancouver, Canada, June 22-26, 2020.
23. Kashif Usmani and Bahram Javidi, “Overview of three-dimensional polarimetric imaging in photon starved conditions,” OSA Imaging and Applied Optics Congress, Vancouver, Canada, June 22-26, 2020.
24. Xin Shen, Artur Carnicer, Bahram Javidi, “3D polarimetric integral imaging in low illumination conditions,” Three-Dimensional Imaging, Visualization, and Display 2020, Proc. SPIE 11402, 27 April - 1 May 2020.
25. Kashif Usmani and Bahram Javidi, “Overview of three-dimensional polarimetric imaging in photon starved conditions,” OSA Imaging and Applied Optics Congress, Vancouver, Canada, June 22-26, 2020.
26. Bahram Javidi, Xin Shen, Adam Markman, Myungjin Cho, Manuel Martinez Corral, Artur Carnicer, Adrian Stern, José Martinez Sotoca, Pedro Latorre-Carmona, Filiberto Pla, “Multidimensional Integral Imaging for Sensing, Visualization, and Recognition in Degraded Environments," OSA Imaging and Applied Optics Congress, Munich, Germany, June 26-29, 2019. **(Invited)**
27. B. Javidi and A. Markman, "Learning in the dark: 3D object recognition in very low illumination conditions using Convolutional Neural Networks and Integral Imaging,” Workshop on Information Optics, Stockholm, Sweden, 1-5 July 2019. (Invited)
28. Bahram Javidi, “Progress in Multi-Dimensional Optical Sensing and Imaging Systems [MOSIS]: From Macro to Micro Scales,” The Spanish Optical Society Annual Meeting, Castelon, Spain, July 3 2018 **[Plenary Address]. No Proceedings Paper.**

Honors, Awards, and Professional Recognition Received:

1. Prof. Javidi was awarded The Optical Society (OSA, Optica) Emmett Leith Medal, 2021

2. The PI, Prof. Bahram Javidi was elected to the National Academy of Inventors (NAI) as a Fellow, 2019-

Prof. Bahram Javidi, University of Connecticut; Email: Bahram.Javidi@UConn.edu

3. Prof. Javidi was awarded The Optical Society (Optica, OSA) C. E. K. Mees Medal (2019)

4. Prof. Javidi was awarded The IEEE Photonics Society William Streifer Scientific Achievement Award (2019)

5. Prof. Javidi is named by The International Society for Optics and Photonics (SPIE) as a Luminary, August 2021

DISTRIBUTION A: Distribution approved for public release.